


Metal-insulator transition in CuIr_2S_4 observed by Cu $K\alpha$ resonant x-ray emission spectroscopyHitoshi Sato ¹, Takuma Matsumoto,² Kazuhiro Maeda,² Yukihiro Taguchi ³, Naomi Kawamura ⁴, and Hiroki Ishibashi ⁵¹*Hiroshima Synchrotron Radiation Center, Hiroshima University, Higashi-Hiroshima 739-0046, Japan*²*Graduate School of Science, Hiroshima University, Higashi-Hiroshima 739-8526, Japan*³*Graduate School of Engineering, Osaka Metropolitan University, Sakai 599-8531, Japan*⁴*Japan Synchrotron Radiation Institute (JASRI), Sayo, Hyogo 679-5198, Japan*⁵*Graduate School of Science, Osaka Metropolitan University, Sakai 599-8531, Japan* (Received 24 June 2022; revised 17 October 2022; accepted 18 October 2022; published 27 October 2022)

We have investigated the Cu-derived electronic structure of iridium spinel compound CuIr_2S_4 with a metal-insulator transition (MIT) at $T_{\text{MIT}} \sim 230$ K by means of high-energy resolution fluorescence-detected x-ray absorption spectroscopy (HERFD-XAS) and Cu $K\alpha$ resonant x-ray emission spectroscopy (RXES) around the Cu K absorption edge. The Cu K HERFD-XAS spectrum in the metallic phase exhibits a peak in the pre-edge region at an incident photon energy of $h\nu_{\text{in}} = 8981$ eV. The peak is ascribed to the Cu $1s$ - $3d$ quadrupole transition and is abruptly shifted to higher energy by about 0.5 eV on going from metallic to insulating phases. The energy shift of the unoccupied Cu $3d$ states is related to the insulator gap formation of CuIr_2S_4 via the hybridization with the Ir $5d$ - S $3p$ bands. A hysteresis behavior is observed in the Cu $1s$ - $3d$ peak intensity between cooling and heating processes around T_{MIT} , consistent with those observed in the transport properties. The abrupt change in the unoccupied Cu $3d$ states across MIT is also clearly detected in the Cu $K\alpha$ RXES spectra.

DOI: [10.1103/PhysRevB.106.155151](https://doi.org/10.1103/PhysRevB.106.155151)**I. INTRODUCTION**

The iridium spinel compound CuIr_2S_4 has attracted much attention because of its metal-insulator transition (MIT) at $T_{\text{MIT}} \sim 230$ K [1,2]. The electrical resistivity of CuIr_2S_4 exhibits metallic behavior above T_{MIT} . After the abrupt increase by three order of magnitude at T_{MIT} , the resistivity continues to increase down to 5 K. A large hysteresis of ~ 10 K around T_{MIT} between cooling and heating processes is observed. The abrupt changes accompanied by the hysteresis are also observed in the magnetic susceptibility [1,2] and thermal conductivity [3].

In the metallic (M) phase, CuIr_2S_4 has a normal cubic spinel structure [1]. The Cu ion at the A site is tetrahedrally coordinated by four S ions, while the Ir ion at the B site is octahedrally coordinated by six S ions. MIT is accompanied by structural distortion to a triclinic structure in the insulating (I) phase [4,5]. It has been proposed that charge ordering of the Ir^{3+} ($5d(t_{2g})^6$) and Ir^{4+} ($5d(t_{2g})^5$) states essentially contributes to MIT. In the I phase, the isomorphous Ir_8^{3+} and Ir_8^{4+} octamers with the Ir biccapped hexagonal ring are formed [4] and $\text{Ir}^{4+} = \text{Ir}^{4+}$ dimerization occurs in the Ir_8^{4+} octamer [see Fig. 7]. This situation can simply be regarded as a formation of a straight $\text{Ir}^{3+} - \text{Ir}^{4+} = \text{Ir}^{4+} - \text{Ir}^{3+}$ chain [6,7]. The $\text{Ir}^{4+} = \text{Ir}^{4+}$ dimerization was indirectly observed by means of x-ray absorption spectroscopy (XAS) at the S K -edge as a peak due to Ir $5d(t_{2g}) - 5d(t_{2g})$ antibonding states via hybridization with the S $3p$ states [6]. In addition to MIT, x-ray irradiation below around 60 K induces a structural transition to tetragonal symmetry while preserving the local triclinic structure [8].

The Ir charge separation in the I phase of CuIr_2S_4 was detected by means of photoemission spectroscopy (PES) with an Al K x-ray source ($h\nu = 1486.6$ eV) for the Ir $4f$ core level [9]. The Ir $4f$ PES spectrum measured at 300 K (M phase) exhibits the $\text{Ir}^{3.5+}$ -originated $4f_{7/2}$ and $4f_{5/2}$ peaks accompanied by satellite structures. With decreasing temperature down to 80 K (I phase), the $4f_{7/2}$ and $4f_{5/2}$ peaks respectively split into two components due to the Ir^{3+} and Ir^{4+} valence states, which indicates Ir^{3+} and Ir^{4+} charge separation. The same behaviors were observed for the Ir $4f$ PES spectra measured using synchrotron radiation in the ultraviolet and soft x-ray regions ($h\nu = 120$ and 630 eV) [10] and hard x-ray region ($h\nu = 6$ keV) [11]. Since the Cu^{2+} -derived satellite structure, on the other hand, is not observed in the Cu $2p$ PES spectrum, the Cu ion is considered to be almost monovalent [9,12], leading to the averaged Ir valence being $3.5+$. The monovalent Cu ion is supported by nuclear magnetic resonance (NMR) experiments [13] and band-structure calculations [14,15]. Therefore it has been considered that the Cu ion does not contribute to MIT in CuIr_2S_4 . Meanwhile, Zn or Ni substitutions for Cu of CuIr_2S_4 suppress MIT; the transition temperature T_{MIT} decreases and the transition becomes obscure with increasing the Zn or Ni concentrations [16,17]. This suggests that the Cu-originated electronic states are also indirectly involved in MIT to some extent. In addition, the Cu^{2+} components have been found in CuS [18] and mineral tetrahedrite $\text{Cu}_{12}\text{Sb}_4\text{S}_{13}$ [19], the Cu valences of which were considered to be Cu^{1+} as CuIr_2S_4 , in the high-energy resolution fluorescence-detected XAS (HERFD-XAS) spectra at the Cu K edge as a pre-edge peak due to $1s$ - $3d$ quadrupole transition.

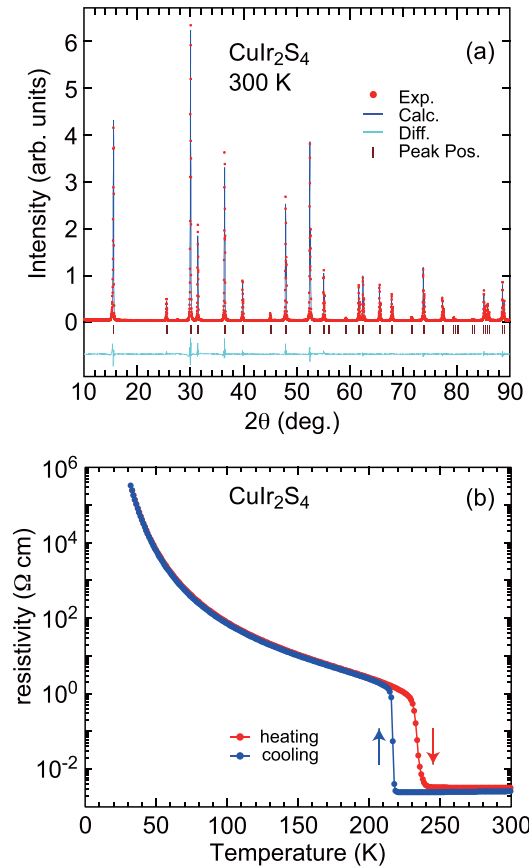


FIG. 1. (a) XRD pattern (red circles) of CuIr_2S_4 measured at 300 K together with the Rietveld refinement profile (blue line), the difference between the observed and calculated profiles (light blue line in the bottom), and the Bragg peak positions (vertical bars). (b) Electrical resistivity of CuIr_2S_4 as a function of temperature.

In this paper, we have investigated the Cu electronic states of CuIr_2S_4 by means of HERFD-XAS and the Cu $K\alpha$ resonant x-ray emission spectroscopy (RXES) around the Cu K absorption edge. Previously, Kijima *et al.* reported the Cu K XAS spectra of CuIr_2S_4 using a laboratory apparatus [20]. The spectra exhibited only a broad absorption structure and almost no temperature dependence was observed. The Cu K absorption edge of CuIr_2S_4 was close to that of Cu_2O (Cu^{1+} ; $3d^{10}$) and the authors concluded that the Cu valence state is monovalent, consistent with the Cu $2p$ PES [9,12] and NMR results [13]. It is well known that the fine structures can be resolved in the HERFD-XAS spectra owing to the small life-time broadening of the final state [21], compared to the conventional XAS with the transmission and total electron yield modes. As a result, we have found that fine feature below the main absorption peak in the HERFD-XAS spectra of CuIr_2S_4 exhibits the change with MIT (see Fig. 2).

II. EXPERIMENTS

The Cu K HERFD-XAS and Cu $K\alpha$ RXES measurements for CuIr_2S_4 were carried out at undulator beamline BL39XU of SPring-8 [22]. A Si 220 double crystal monochromator was used to monochromatize undulator beam and the beam was

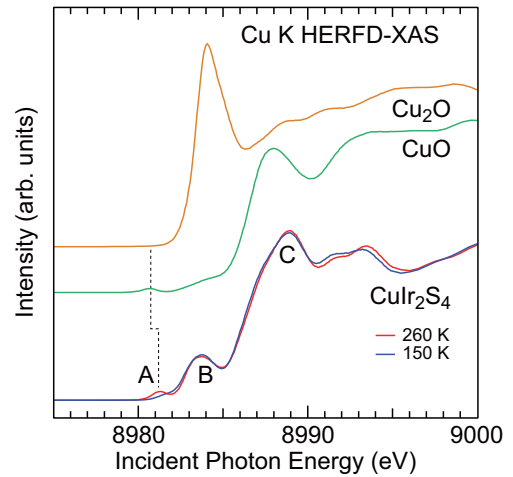


FIG. 2. Cu K HERFD-XAS spectra of CuIr_2S_4 measured at 260 K in the M phase and at 150 K in the I phase in comparison with those of CuO (Cu^{2+} ; $3d^9$) and Cu_2O (Cu^{1+} ; $3d^{10}$) measured at 300 K.

focused onto the sample surface with size of $0.1(\text{horizontal}) \times 0.3(\text{vertical}) \text{ mm}^2$. For the Cu $K\alpha$ RXES, emitted photons from the sample were monochromatized and focused by five Si 444 spherically bent crystals and detected with a two-dimensional pixel detector (PILATUS). The HERFD-XAS spectra were collected by measuring the fluorescence intensity of the Cu $K\alpha_1$ line with photon energy of $h\nu_{\text{out}} = 8047.78 \text{ eV}$, emitted following the Cu $1s$ absorption. The total energy resolution was about 1.0 eV. The temperature of the sample was controlled using a closed-circuit He cryostat and a heater attached to the sample holder.

Polycrystalline samples of CuIr_2S_4 were synthesized by a solid reaction method [8]. Mixtures of Cu, Ir, and S powders were heated in an evacuated quartz tube at 850°C for seven days. The sample was ground and pressed into a pellet, and then sintered in vacuum for three days. The grown sample was characterized by Cu $K\alpha$ x-ray powder diffraction (XRD) measurements at 300 K and electrical resistivity measurements as shown in Figs. 1(a) and 1(b), respectively. No impurity phase was found in the XRD pattern. The Rietveld refinement of the XRD pattern was carried out using the RIETAN-FP program [23]. MIT with hysteresis behavior in the resistivity in Fig. 1(b) was observed around 230 K, consistent with previous results [1,2].

III. RESULTS

Figure 2 shows HERFD-XAS spectra at the Cu K absorption edge of CuIr_2S_4 measured at 260 K in the M phase and at 150 K in the I phase. The two spectra have been normalized with the integrated intensity in the incident photon energy region of $h\nu_{\text{in}} = 8975 - 9020 \text{ eV}$. In comparison with the previous Cu K XAS spectra measured with a laboratory apparatus [20], several fine structures are well resolved in the present HERFD-XAS spectra. The spectrum at 260 K exhibits a main peak (C in the figure), so called white line, at $h\nu_{\text{in}} = 8989 \text{ eV}$ with a shoulder at the lower energy by 1.5 eV. We find two peaks at 8981 eV (A) and 8984 eV

(B) below the main peak, while two structures at 8991.5 and 8993.5 eV above the main peak. The HERFD-XAS spectra of CuO and Cu₂O, which are known as typical Cu²⁺ ($3d^9$) and Cu¹⁺ ($3d^{10}$) reference materials, respectively, measured at 300 K are also presented in Fig. 2. The CuO spectrum shows a pre-edge peak at 8981 eV, while the Cu₂O spectrum no structure below a main peak at 8984 eV. It is well known that the pre-edge peak of CuO is ascribed to the Cu $1s$ - $3d$ quadrupole transition [24,25]. Peak A in the CuIr₂S₄ spectra is expected to correspond to the pre-edge peak at 8981 eV of the CuO spectrum judging from their energy positions. The pre-edge peak is also observed in the Cu $K\beta_1$ fluorescence spectra of CuS taken by measuring the Cu $K\beta_1$ fluorescence intensity, and the peak is ascribed to the Cu $1s$ - $3d$ quadrupole transition [18]. Based on these assignments for CuO [24,25] and CuS [18], we ascribe peak A in the CuIr₂S₄ spectra to the Cu $1s$ - $3d$ quadrupole transition. The appearance of peak A, thus, indicates that the Cu $3d$ states are not fully occupied but they are partially unoccupied. In words with the valence, the Cu valence is not exactly Cu¹⁺ but a small amount of the Cu²⁺ components exists in the M phase. Since the Cu ion is tetrahedrally surrounded by four S ions, $3d$ holes are doped into the t_2 orbitals. On the other hand, peak B as well as the main peak C are attributed to the Cu $1s$ - $4p$ dipole transition, in comparison with the HERFD-XAS spectra of CuS [18] and mineral tetrahedrite Cu₁₂Sb₄S₁₃ [19]. We find some differences between the spectra at 260 and 150 K across MIT in the energy range extending above 8990 eV from 8980 eV. In particular, the pre-edge peak assigned to the $1s$ - $3d$ quadrupole transition is reduced at 150 K, indicating that the Cu $3d$ states vary between the M and I phases. Hereafter, we focus on the temperature change in the spectral feature in the pre-edge region.

Figure 3(a) shows the temperature dependence of the pre-edge region of the Cu K HERFD-XAS spectra of CuIr₂S₄ taken upon cooling from 300 to 10 K. It is noticed that the spectral feature abruptly changes between 260 and 190 K across MIT. The Cu $1s$ - $3d$ peak at $h\nu_{\text{in}} = 8981.2$ eV (A) clearly observed in the spectra above 260 K, suddenly disappears below 190 K. The leading edge of the spectra is shifted to higher energy and becomes less steep. The spectral feature is almost the same in the M phase at above 260 K, and so is in the I phase below 190 K. Below 190 K, the broad shoulder appears between 8981 and 8982 eV as labeled with A' in the figure, which is overlapped with the tail of the Cu $1s$ - $4p$ peak at 8983.6 eV (B). A feature corresponding to this shoulder structure is observed as a sharp peak in the Cu $K\alpha$ RXES spectra measured at $h\nu_{\text{in}} = 8981.0$ and 8981.5 eV as will be shown later [see Figs. 5(d) and 5(e)]. The $1s$ - $3d$ peak in the M phase seems to be shifted to higher energy by about 0.5 eV in the I phase, which indicates that the Cu $3d$ unoccupied states are shifted to higher energy across MIT. The observed energy shift is consistent with an energy gap ΔE of 0.5–0.75 eV in the density of states (DOS) at E_F [26,27]. The temperature dependence due to the structural transformation induced by x-ray irradiation between 90 and 10 K [8], was not clearly observed in the present measurements within the experimental accuracy.

Figure 3(b) exhibits the detailed temperature dependencies of the HERFD-XAS spectra with changing temperature

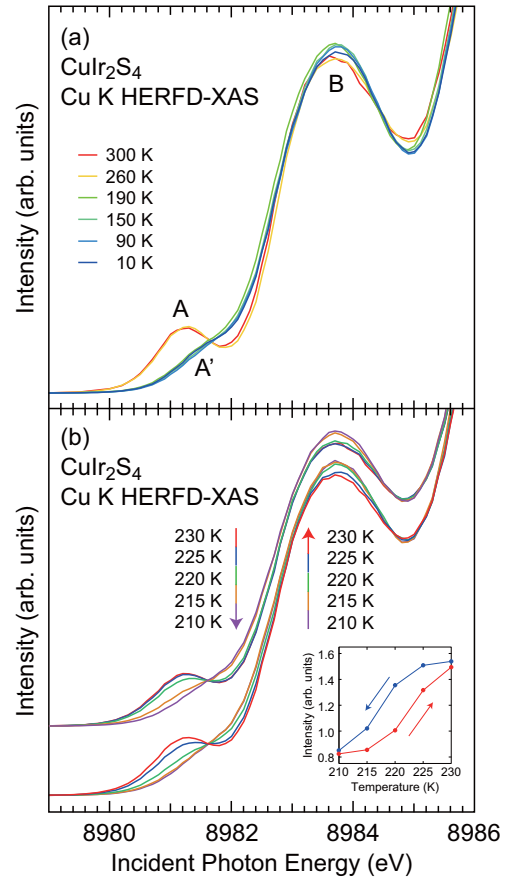


FIG. 3. (a) Temperature dependence of the pre-edge region of Cu K HERFD-XAS spectra of CuIr₂S₄ measured between 300 and 10 K. (b) The same as (a) measured between 230 and 210 K with decreasing (upper part) and increasing (lower part) temperature. Inset shows the intensities at $h\nu_{\text{in}} = 8981.2$ eV as a function of temperature for the cooling (blue) and heating (red) processes.

in steps of 5 K around T_{MIT} . The spectra in the upper and lower parts of the figure were measured with decreasing and increasing temperature, respectively. The Cu $1s$ - $3d$ peak at $h\nu_{\text{in}} = 8981.2$ eV is gradually reduced upon cooling from 220 to 215 K, while enhanced upon heating from 220 to 225 K. The peak intensities are plotted as a function of temperature in inset of Fig. 3(b), where a clear hysteresis behavior is shown. Such a hysteresis behavior is consistent with those observed in the electrical resistivity in Fig. 1(b), magnetic susceptibility [1,2], and thermal conductivity [3], and indicates that the change in the $1s$ - $3d$ peak is obviously related to MIT in CuIr₂S₄ and that the Cu $3d$ unoccupied states are modified in accord with MIT [28]. Hysteresis behavior such as that seen in Fig. 3(b) has not been observed in x-ray spectroscopic measurements for CuIr₂S₄, so far, and the present results are the first observation of this.

In order to further examine the change in the Cu $3d$ states across MIT in CuIr₂S₄, we have carried out Cu $K\alpha$ RXES around the Cu K absorption region as shown in Figs. 4 and 5. In Fig. 4(b), we show a series of RXES spectra measured at 300 K in the M phase with $h\nu_{\text{in}}$ from 8975 eV well below the Cu K absorption edge to 8990 eV well above the

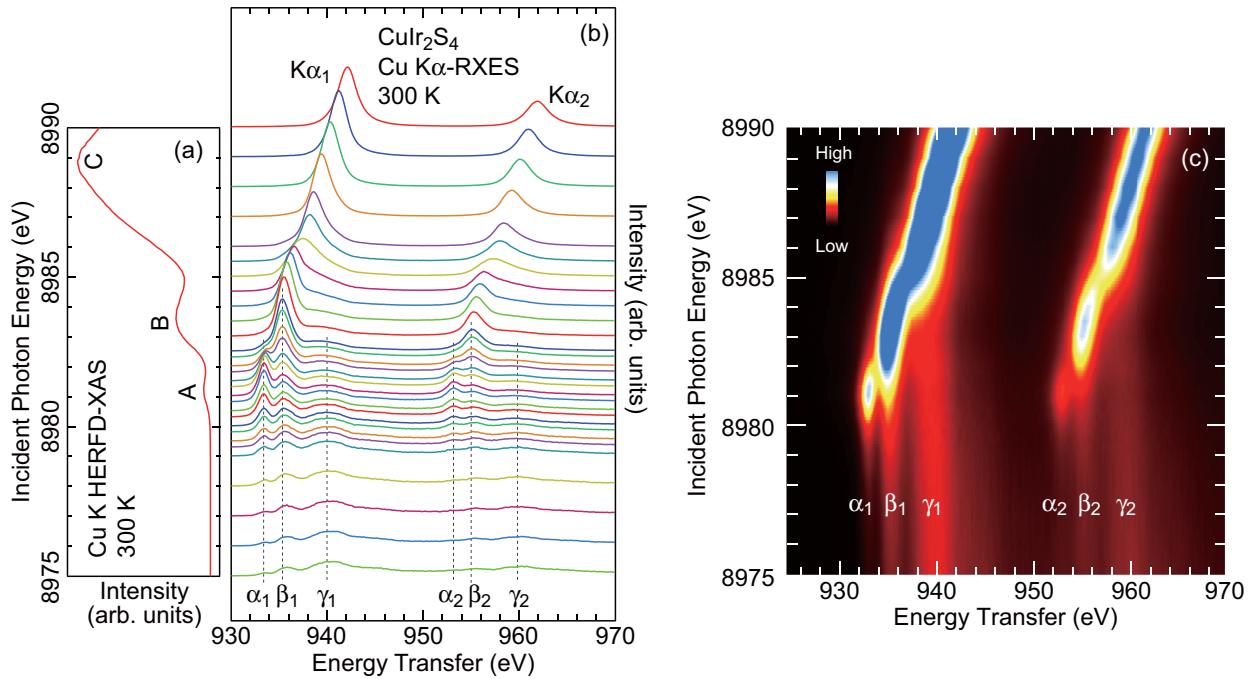


FIG. 4. (a) Cu K HERFD-XAS spectrum of CuIr_2S_4 measured at 300 K for RXES spectra in (b). (b) $h\nu_{\text{in}}$ -dependent Cu $K\alpha$ RXES spectra of CuIr_2S_4 measured at 300 K around the Cu K absorption edge. Horizontal axis is an energy transfer defined by $\Delta h\nu = h\nu_{\text{in}} - h\nu_{\text{out}}$. Vertical offset of each spectrum is scaled to $h\nu_{\text{in}}$ axis in HERFD-XAS spectrum in (a). (c) Two-dimensional image plot of RXES spectra in (b).

edge. The spectra have been normalized with the incident photon intensity. Energy transfer for the horizontal axis is defined as the energy difference between the incident and emitted photon energies; $\Delta h\nu = h\nu_{\text{in}} - h\nu_{\text{out}}$. The vertical offset of each RXES spectrum is scaled to the $h\nu_{\text{in}}$ axis of the HERFD-XAS spectrum in Fig. 4(a). The RXES spectra split into the $K\alpha_1$ region of $\Delta h\nu = 930$ –950 eV and $K\alpha_2$ region of $\Delta h\nu = 950$ –970 eV. Almost the same $h\nu_{\text{in}}$ dependence is detected in both regions. The spectral feature significantly changes depending on $h\nu_{\text{in}}$, in particular, in the pre-edge region of the HARFD-XAS spectrum. In the bottom RXES spectrum at $h\nu_{\text{in}} = 8975$ eV, three characteristic structures labeled with α_1 , β_1 , and γ_1 in the figure, are found at around $\Delta h\nu = 933$, 935, and 940 eV in the $K\alpha_1$ region, respectively. The corresponding structures α_2 , β_2 , and γ_2 are observed at around $\Delta h\nu = 953$, 955, and 960 eV in the $K\alpha_2$ region. The energy transfers of these structures remain constant below $h\nu_{\text{in}} \sim 8982$ eV, indicating that these structures are ascribed to the Raman components. Above $h\nu_{\text{in}} \sim 8982$ eV, on the other hand, two prominent peaks, which move to higher energy transfer with increasing $h\nu_{\text{in}}$, are attributed to the $K\alpha_1$ and $K\alpha_2$ fluorescence lines at the constant emission energies of $h\nu_{\text{out}} = 8047.8$ and 8027.8 eV, respectively.

Peak at the lowest energy transfer of $\Delta h\nu = 933$ eV (α_1) is gradually enhanced with increasing $h\nu_{\text{in}}$ from 8975 eV and become the most prominent around 8981 eV just at the Cu $1s$ – $3d$ pre-edge peak of the HERFD-XAS spectrum [A in Fig. 4(a)]. Peak α_1 disappears with further increasing $h\nu_{\text{in}}$. The enhancement around the $1s$ – $3d$ HERFD-XAS peak indicates that the peak α_1 is related to the Cu $3d$ unoccupied states. After the enhancement of peak α_1 , peak β_1 is enhanced around the $1s$ – $4p$ HERFD-XAS peak at $h\nu_{\text{in}} = 8984$ eV [B in Fig. 4(a)]. Peak β_1 continuously connects

to the $K\alpha_1$ fluorescence line with further increasing $h\nu_{\text{in}}$. The same behavior is detected for the α_2 and β_2 peaks in the $K\alpha_2$ region. This is clearly seen in the two-dimensional plot of the RXES intensity versus $\Delta h\nu$ and $h\nu_{\text{in}}$ displayed in Fig. 4(c). The enhancement of the Cu $3d$ -related RXES peaks α_1 and α_2 are noticed around $\Delta h\nu = 933$ eV and $h\nu_{\text{in}} = 8981$ eV, and $\Delta h\nu = 953$ eV and $h\nu_{\text{in}} = 8981$ eV, respectively.

Figure 5 shows the temperature dependences of the Cu $K\alpha$ RXES spectra of CuIr_2S_4 taken at selected incident photon energies in the $1s$ – $3d$ pre-edge peak region of the Cu K HERFD-XAS spectra. The RXES spectra have been normalized to the incident photon intensity. The incident photon energies $h\nu_{\text{in}}$ for the RXES spectra are indicated by vertical bars on the HERFD-XAS spectra in inset of each figure. In the RXES spectra measured at $h\nu_{\text{in}} = 8979.5$ eV [Fig. 5(a)], three Raman components α_1 , β_1 , and γ_1 are observed at $\Delta h\nu = 933.4$, 935, and 940 eV in the $K\alpha_1$ region, and α_2 , β_2 , and γ_2 at $\Delta h\nu = 953.2$, 955, and 960 eV in the $K\alpha_2$ region, as described before. These structures are observed up to $h\nu_{\text{in}} = 8981.5$ eV [Fig. 5(e)], although their relative intensity varies depending on $h\nu_{\text{in}}$. Among three structures, the lowest-lying peaks at $\Delta h\nu = 933.4$ and 953.2 eV (α_1 and α_2) are abruptly reduced from 260 to 190 K across MIT. In the RXES spectra below 190 K at $h\nu_{\text{in}} = 8979.5$ eV, the α'_1 and α'_2 shoulders are still visible near the α_1 and α_2 peaks, as indicated by vertical bars in Fig. 5(a). They become more distinct with increasing $h\nu_{\text{in}}$, being best seen for $h\nu_{\text{in}} = 8981.0$ and 8981.5 eV [Figs. 5(d) and 5(e)]. In particular, the shoulder α'_1 is observed as a clear peak. Figure 6 shows the enlarged RXES spectra of Fig. 5(e) in the α_1 , α'_1 , and β_1 peak region measured at 260 and 190 K, superimposed with a fit by three Voigt functions. Peak α_1 is located at $\Delta h\nu = 933.45$ eV, while

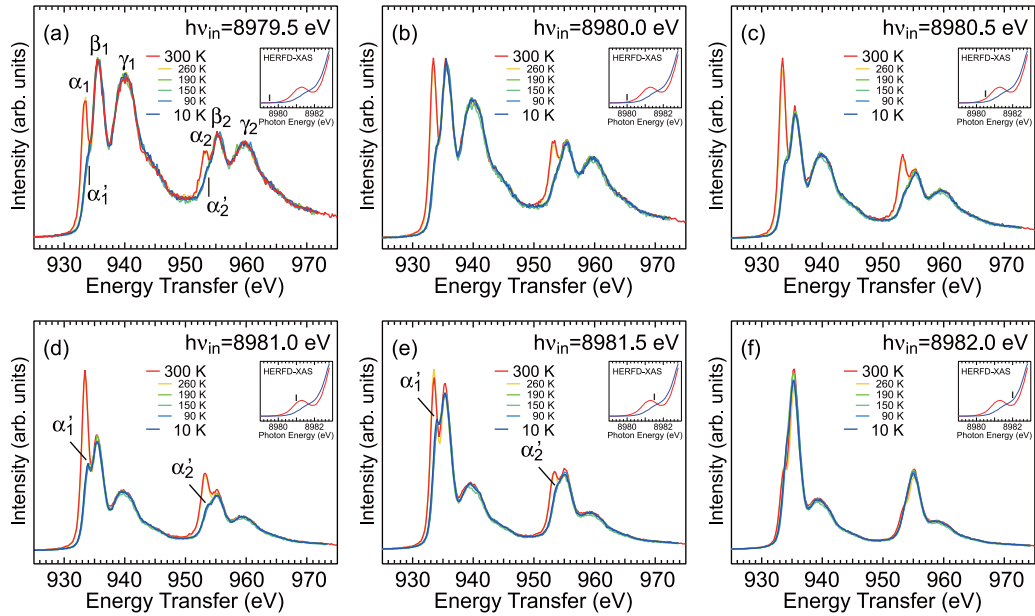


FIG. 5. Temperature-dependent Cu $K\alpha$ RXES spectra of CuIr_2S_4 measured between 300 and 10 K with $h\nu_{\text{in}}$ of (a) 8979.5, (b) 8980.0, (c) 8980.5, (d) 8981.0, (e) 8981.5, and (f) 8982.0 eV. The incident photon energies $h\nu_{\text{in}}$ are indicated by vertical bars on the HERFD-XAS spectra measured at 260 K (red curve) and 150 K (blue curve) in respective insets.

peak α'_1 at 933.91 eV. Note that peak α'_1 is shifted to higher energy transfer by about 0.5 eV in comparison with peak α_1 .

The temperature dependences of the intensity ratios between the α_1 and α'_1 peaks and between the α_2 and α'_2 peaks in the RXES spectra can be explained by the HERFD-XAS intensities at the excitation energy $h\nu_{\text{in}}$. In each inset in Fig. 5, the HERFD-XAS spectra measured at 260 K in the M phase and at 150 K in the I phase are displayed by red and blue curves, respectively. From $h\nu_{\text{in}} = 8980.0$ to 8981.5 eV [Figs. 5(b)–5(e)], the HERFD-XAS intensity is lower in the I phase due to the reduction of the Cu $1s-3d$ peak intensity. As described before, the α_1 and α_2 peaks of the RXES spectra

are enhanced around the Cu $1s-3d$ peak of the HERFD-XAS spectrum [A in Figs. 3(a) or 4(a)], and are reduced in the I phase. On the other hand, the leading edge of the HERFD-XAS spectrum in the I phase is shifted to higher energy and the spectrum starts to rise just at $h\nu_{\text{in}} = 8981.0$ eV [inset in Fig. 5(d)], where the α'_1 component is detected as clear peak. Therefore the α'_1 and α'_2 peaks are closely related to the broad shoulder of the HERFD-XAS spectra indicated by A' in Figs. 3(a) or 4(a). Note that peak α'_1 is located at an energy transfer about 0.5 eV higher than peak α_1 as seen in Fig. 6. This indicates that the Cu $3d$ empty states are shifted to higher energy in the I phase. Again, the observed energy shift is in good agreement with the energy gap value [26,27].

The HERFD-XAS intensity at $h\nu_{\text{in}} = 8982.0$ eV becomes higher in the I phase compared to the M phase as shown in inset in Fig. 5(f) or Fig. 3. However, the large HERFD-XAS peak B at $h\nu_{\text{in}} = 8984$ eV derived from the Cu $1s-4p$ transition is overlapped around $h\nu_{\text{in}} = 8982.0$ eV. As a result, the α'_1 and α'_2 peaks of the RXES spectra become less visible due to the existence of the β_1 and β_2 peaks, which are related to the Cu $4p$ unoccupied states. The α_1 and α_2 peaks still appear as shoulders in the spectra recorded above 260 K at $h\nu_{\text{in}} = 8982.0$ eV. From this fact, the Cu $3d$ unoccupied states in the M phase contribute to the HERFD-XAS intensity at $h\nu_{\text{in}} = 8982.0$ eV.

The assignments of the α , α' , and β peaks, where α represents both α_1 and α_2 and the same for α' and β , are interpreted also from arguments by Hayashi *et al.* [29,30]. They showed that the XAS spectra with suppressed life-time broadening can be obtained using the $h\nu_{\text{in}}$ -dependent RXES spectra based on the Tulkki-Åberg equation [31], which is reduced from the Kramers-Heisenberg equation, and that a correspondence is found between the RXES and XAS features. According to their results on CuO [29], the three components α , α' , and β in the RXES spectra correspond to the HERFD-XAS peaks

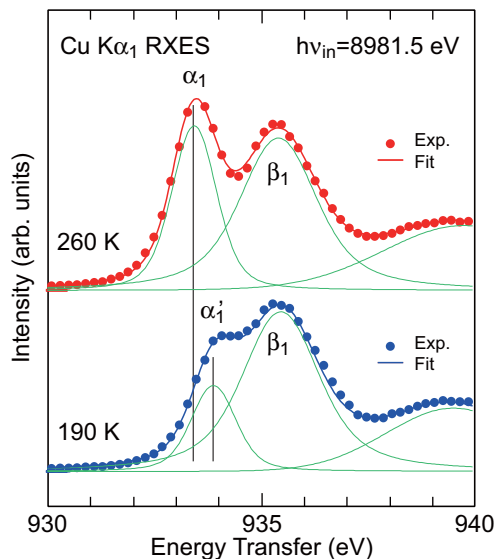


FIG. 6. Cu $K\alpha_1$ RXES spectra of CuIr_2S_4 measured at 260 and 190 K with $h\nu_{\text{in}} = 8981.5$ eV and fits with three Voigt functions.

A, A', and B, respectively. In the same way, the broad γ peaks correspond to the HERFD-XAS main peak C.

IV. DISCUSSION

The HERFD-XAS and Cu $K\alpha$ RXES results at the Cu K absorption edge reveal that a part of the Cu $3d$ states of CuIr_2S_4 is unoccupied. On the other hand, the Cu $2p$ PES spectra of CuIr_2S_4 exhibit no Cu^{2+} -derived satellite structures [9,12] as observed for the typical Cu^{2+} compound CuO [24,25]. It is well known that the satellite peaks are attributed to the $2p^53d^9$ final states [32]. The appearance of the satellite structure reflects the localized character of the Cu $3d$ states of CuO. From the HERFD-XAS and RXES results combined with the Cu $2p$ PES results, the Cu $3d$ unoccupied states of CuIr_2S_4 are considered to be delocalized compared to those of CuO.

The feature and temperature dependence of the Cu K HERFD-XAS spectra of CuIr_2S_4 in Fig. 3 are very similar to those of the XAS spectra at the S K -edge taken at 239 K in the M phase and at 225 K in the I phase measured with the fluorescence and transmission modes [see Fig. 2 in Ref. [6]]. The S K XAS spectrum at 239 K exhibits a low-intensity peak at $h\nu_{\text{in}} = 2470.3$ eV and a high-intensity peak at 2472.5 eV. At 225 K (I phase), the low-intensity peak is shifted to higher energy by 0.5 eV across MIT, while the high-intensity peak shows almost no energy shift. The authors interpreted the spectra based on the simple molecular orbital electronic structure composed of the Ir and S ions [see Fig. 4 in Ref. [6]]. The Ir $5d$ states are hybridized with the S $3p$ states and the S K XAS spectra reflect the Ir $5d$ unoccupied states through the hybridization. In the M phase, the low-intensity peak is attributed to unoccupied π^* antibonding orbitals composed of the S $3p$ and Ir $5d(t_{2g})$ states, and the high-intensity peak to σ^* antibonding orbitals composed of the S $3p$ and Ir $5d(e_g)$ states. Note that the all Ir ions take the valence of $\text{Ir}^{3.5+}(t_{2g}^{5.5})$ and the π^* bands are $\frac{3}{4}$ -filled at E_F , making the system metallic. In the I phase, on the other hand, the Ir ions form the repeated $\text{Ir}^{3+}(t_{2g}^6) - \text{Ir}^{4+}(t_{2g}^5) = \text{Ir}^{4+}(t_{2g}^5) - \text{Ir}^{3+}(t_{2g}^6)$ chain with the $\text{Ir}^{4+} = \text{Ir}^{4+}$ dimer. At the $\text{Ir}^{4+} = \text{Ir}^{4+}$ dimer site, the highest-lying $5d(t_{2g})$ empty orbital points directly toward the Ir ion and hybridizes with the $5d(t_{2g})$ empty orbital of the partner Ir^{4+} ion. As a result, the $\frac{3}{4}$ -filled π^* bands in the M phase are split into the occupied lower $d_{||}$ bands and unoccupied $d_{||}^*$ bands at the $\text{Ir}^{4+} = \text{Ir}^{4+}$ dimer site, forming an energy gap at E_F . On going from the M to I phases, the empty part of the π^* bands are pushed up to the empty $d_{||}^*$ bands, causing the energy shift of the low-intensity peak of the S K XAS spectra. The peak A of the Cu K HERFD-XAS spectra of CuIr_2S_4 in Fig. 3 corresponds to the low-intensity peak at 239 K of the S K XAS spectrum, A' to the peak at 225 K, and B to the high-intensity peak. In comparison with the S K XAS spectra, these peaks A, A', and B are attributed to the empty π^* bands, $d_{||}^*$ bands, and σ^* bands, respectively. It is considered that the Cu $3d$ states are indirectly involved in MIT in CuIr_2S_4 through the hybridization with the Ir $5d-3p$ bands due to their delocalized character.

This finding is also supported from the fact that the spectral change in the present Cu $K\alpha$ RXES across MIT in CuIr_2S_4

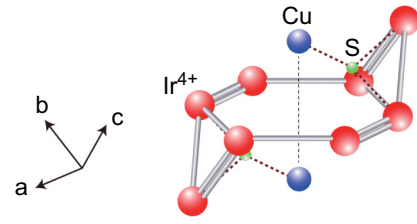


FIG. 7. Ir^{4+} octamer [4], the closest Cu ions to the octamer, and a portion of the S ions. $\text{Ir}^{4+} = \text{Ir}^{4+}$ dimers are displayed with double sticks. Hexagonal ring lies in the $(11\bar{1})$ plane.

is similar to that observed in the Ir $L\alpha_2$ RXES [27]. The Ir-derived electronic structure of CuIr_2S_4 was investigated by means of the HERFD-XAS and Ir $L\alpha_2$ RXES around the Ir L_3 absorption edge [27]. The Ir $L\alpha_2$ RXES spectra measured at $h\nu_{\text{in}} = 11215$ eV, which is 3 eV below the Ir L_3 HERFD-XAS peak, show a slight change between above and below MIT. In the RXES spectrum at 250 K (M phase), the main peak appears at $\Delta h\nu = 2118.5$ eV ($h\nu_{\text{out}} = 9096.5$ eV) with a shoulder at $\Delta h\nu = 2117$ eV ($h\nu_{\text{out}} = 9098$ eV). The shoulder structure has almost vanished at 215 K (I phase) and the RXES spectrum appeared to become a single peak. The authors fitted both the spectra at 250 and 215 K using two Voigt functions, taking into account the shoulder component observed at 250 K. The fitted results showed that the main peak exhibits almost no shift, while the shoulder is shifted to the higher $\Delta h\nu$ (lower $h\nu_{\text{out}}$) by $\Delta E \sim 0.55$ eV. The authors attributed the main peak and shoulder to the Ir $5d(e_g)$ and $5d(t_{2g})$ components, respectively. Based on the band-structure calculations using density functional theory [14,15], they pointed out that the opening of an insulating gap occurs due to the shift of the empty Ir $5d(t_{2g})$ band.

The β peak of the Cu $K\alpha$ RXES spectra in Fig. 5(a) corresponds to the main peak of the Ir $L\alpha_2$ RXES spectra, while the α peak corresponds to the shoulder structure in the M phase [27]. The energy shift of the shoulder structure of the Ir $L\alpha_2$ RXES spectra, which was only indicated by the fits [27], is clearly detected in our Cu $K\alpha$ RXES spectra as the α' peak in Figs. 5(d) and 5(e). The energy shift values (~ 0.5 eV) deduced from RXES using Cu $K\alpha$ (this work) and Ir $L\alpha_2$ [27] are in good agreement.

The present results of the Cu K HERFD-XAS and Cu $K\alpha$ RXES in comparison with the S K XAS [6] and Ir $L\alpha_2$ RXES results [27], respectively, indicate that the Cu $3d$ states are indirectly involved in MIT in CuIr_2S_4 through the hybridization with the Ir $5d(t_{2g})$ and S $3p$ states. The hybridization is also supported by the band-structure calculation for CuIr_2S_4 [14,15], where the low but finite Cu $3d$ DOS exists above E_F and the DOS feature is similar to a shape of the Cu K HERFD-XAS spectra. In addition, the Cu $3d$ DOS feature is similar to the Ir $5d$ and S $3p$ DOS features. As pointed by Radaelli *et al.* [4], the Ir^{3+} and Ir^{4+} ions respectively form the isomorphic octamers in the I phase, which consist of a hexagonal ring with two triangles as shown in Fig. 7. The two triangles share the opposite sides of the hexagonal ring and point to obliquely upward and downward directions. The closest Cu ions to the Ir ions are located just above and below the center of the hexagonal ring and are considered to interact

with the upward and downward triangles, respectively, as well as the hexagonal rings, through the S ions. The Ir^{4+} octamer has four $\text{Ir}^{4+} = \text{Ir}^{4+}$ dimer bonds as shown with double sticks in the figure. The Cu ions connect with all Ir^{4+} ions including the dimerized ones in the octamer by sharing the S ions. The S ion shown in Fig. 7 forms bonds with one Cu ion, two dimerized Ir ions and one nondimerized Ir ion. The $3d$ states of the Cu ions situated just above and below the hexagonal rings are expected to contribute to the unoccupied $d_{||}^*$ bands at the $\text{Ir}^{4+} = \text{Ir}^{4+}$ dimer and to the gap formation mediated by the S ions. In line with the same arguments, the Cu $4p$ states are also included in the σ^* antibonding bands.

The low-intensity peak of the S K XAS spectrum at 239 K is shifted to higher energy and is increased in intensity at 225 K [6], while the pre-edge peak A in the Cu K HERFD-XAS spectra in the M phase is more remarkable in comparison with the shoulder A' in the I phase [see Fig. 3]. Note that the low-intensity peak of the S K XAS spectrum at 239 K corresponds to the pre-edge peak A in the Cu K HERFD-XAS spectra and that at 225 K to the shoulder A' . The difference between the S and Cu spectra would suggest that the Cu $3d$ hybridization with the Ir $5d-S$ $3p$ bands becomes weak in the I phase.

Finally, we would like to emphasize that the Cu K HERFD-XAS and $K\alpha$ RXES are sensitive to the Cu $3d$ empty states in comparison with the Cu $2p$ PES. The similar changes in the Cu K HERFD-XAS and $K\alpha$ RXES spectra across MIT in CuIr_2S_4 as in Figs. 3(a) and 5, were obtained for mineral tetrahedrite $\text{Cu}_{12}\text{Sb}_4\text{S}_{13}$ [19], which undergoes a metal-semiconductor transition (MST) at $T_{\text{MST}} = 85$ K [33,34]. Although it is expected that Cu^{2+} is related to MST in $\text{Cu}_{12}\text{Sb}_4\text{S}_{13}$, the Cu^{2+} satellite features are not detected in the Cu $2p$ PES [35]. On the other hand, the Cu $3d$ unoccupied states are observed in the Cu K HERFD-XAS and $K\alpha$ RXES spectra of $\text{Cu}_{12}\text{Sb}_4\text{S}_{13}$ [19] as in the present experiments. The Cu $3d$ -derived peak is shifted to higher energy below T_{MST} , which shows that MST in $\text{Cu}_{12}\text{Sb}_4\text{S}_{13}$ is caused by the shift of the Cu $3d$ states. In case of CuIr_2S_4 , the Ir charge ordering and resultant electronic structure mainly contributes to MIT, while the Cu $3d$ states are also expected to be related to MIT via the hybridization with the Ir $5d-S$ $3p$ bands as revealed from the HERFD-XAS and RXES results.

Among CuM_2S_4 ($M = \text{Co}, \text{Rh}, \text{Ir}$), only CuIr_2S_4 undergoes MIT. According to the band-structure calculation, the total DOS's at E_F decreases on going from $M = \text{Co}$ to Rh

and to Ir [36]. The suppression of MIT by the Zn or Ni substitutions for Cu of CuIr_2S_4 [16,17] might be related to the increase in the $3d$ DOS at E_F with increasing the Zn or Ni substitutions. The Cu K HERFD-XAS and $K\alpha$ RXES for $\text{Cu}_{1-x}\text{Zn}_x\text{Ir}_2\text{S}_4$ and $\text{Cu}_{1-x}\text{Ni}_x\text{Ir}_2\text{S}_4$ are desired to reveal the role of the Cu $3d$ states in MIT in CuIr_2S_4 .

V. SUMMARY

We have investigated the Cu-derived electronic structure of CuIr_2S_4 by means of the HERFD-XAS and Cu $K\alpha$ RXES around the Cu K absorption edge. The HERFD-XAS spectra in the M phase exhibit the peak in the pre-edge region, assigned to the Cu $1s-3d$ quadrupole transition. This peak is shifted to higher energy on going from the M to I phases, which indicates that the Cu $3d$ unoccupied states are shifted to higher energy. Between the cooling and heating processes, the hysteresis behavior is observed in the HERFD-XAS spectra as is observed in the electrical resistivity, magnetic susceptibility [1,2], and thermal conductivity [3] measurements. The energy shift of the Cu $3d$ unoccupied states across MIT is also observed in the RXES spectra. The energy shift of about 0.5 eV is in agreement with the energy gap of $\Delta E \sim 0.5-0.75$ eV at E_F in the I phase [26,27]. The changes in the Cu K HERFD-XAS and Cu $K\alpha$ RXES spectra across MIT are similar to those of S K XAS [6] and Ir $L\alpha_2$ RXES spectra [27]. These similarities indicate that the Cu $3d$ states hybridize with the Ir $5d$ bands by sharing the S ions with the Ir ions. Due to the delocalized character of the Cu $3d$ states, the Cu^{2+} -originated satellite structures are not observed in the Cu $2p$ PES [9,12]. We conclude that the energy shift of the Cu $3d$ empty states is related to the insulator gap formation via the Ir $5d(t_{2g})-S$ $3p$ bands and that the Cu $3d$ states are also involved in MIT in CuIr_2S_4 .

ACKNOWLEDGMENTS

The authors are grateful to T. Fumiyama for experimental support. They also thank J. Ghijsen for critical reading of the manuscript. The experiments at BL39XU of SPring-8 were performed under the approval of the Japan Synchrotron Radiation Research Institute (JASRI) (Proposal No. 2018B1330, No. 2019A1276, No. 2021A1211, No. 2021A2072, No. 2021B2090, and No. 2022A1280).

- [1] T. Furubayashi, T. Matsutomo, T. Hagino, and S. Nagata, Structural and magnetic studies of metal-insulator transition in thiospinel CuIr_2S_4 , *J. Phys. Soc. Jpn.* **63**, 3333 (1994).
- [2] T. Hagino, T. Tojo, T. Atake, and S. Nagata, Metal-insulator transition at 230 K in a new thiospinel CuIr_2S_4 , *Philos. Mag. B* **71**, 881 (1995).
- [3] M. Ito, K. Sonoda, and S. Nagata, Temperature dependence of thermodynamic properties of spinel CuIr_2S_4 , *Solid State Commun.* **265**, 23 (2017).
- [4] P. G. Radaelli, Y. Horibe, M. J. Gutmann, H. Ishibashi, C. H. Chen, R. M. Ibberson, Y. Koyama, Y.-S. Hor, V. Kiryukhin, and S.-W. Cheong, Formation of isomorphous Ir^{3+} and Ir^{4+} octamers and spin dimerization in the spinel CuIr_2S_4 , *Nature (London)* **416**, 155 (2002).
- [5] H. Ishibashi, T. Sakai, and K. Nakahigashi, X-ray diffraction study on spinel compound CuIr_2S_4 with metal-insulator transition, *J. Magn. Magn. Mater.* **226-230**, 233 (2001).
- [6] M. Croft, W. Caliebe, H. Woo, T. A. Tyson, D. Sills, Y. S. Hor, S.-W. Cheong, V. Kiryukhin, and S.-J. Oh, Metal-insulator transition in CuIr_2S_4 : XAS results on the electronic structure, *Phys. Rev. B* **67**, 201102(R) (2003).
- [7] D. I. Khomskii and T. Mizokawa, Orbitally Induced Peierls State in Spinels, *Phys. Rev. Lett.* **94**, 156402 (2005).

- [8] H. Ishibashi, T. Y. Koo, Y. S. Hor, A. Borissov, P. G. Radaelli, Y. Horibe, S.-W. Cheong, and V. Kiryukhin, X-ray-induced disordering of the dimerization pattern and apparent low-temperature enhancement of lattice symmetry in spinel CuIr_2S_4 , *Phys. Rev. B* **66**, 144424 (2002).
- [9] K. Takubo, S. Hirata, J.-Y. Son, J. W. Quilty, T. Mizokawa, N. Matsumoto, and S. Nagata, X-Ray Photoemission Study of CuIr_2S_4 : Ir^{3+} - Ir^{4+} Charge Ordering and the Effect of Light Illumination, *Phys. Rev. Lett.* **95**, 246401 (2005).
- [10] H.-J. Noh, E.-J. Cho, H.-D. Kim, J.-Y. Kim, C.-H. Min, B.-G. Park, and S.-W. Cheong, Ir^{3+} - Ir^{4+} charge disproportionation in spinel CuIr_2S_4 investigated by synchrotron-radiation photoemission spectroscopy, *Phys. Rev. B* **76**, 233106 (2007).
- [11] Y. Taguchi, K. Yamamoto, K. Mimura, K. Ichikawa, K. Kitamoto, O. Aita, H. Ishibashi, Y. Takata, K. Horiba, S. Shin, M. Yabashi, K. Tamasaku, Y. Nishino, D. Miwa, T. Ishikawa, E. Ikenaga, and K. Kobayashi, Ir $4f$ hard x-ray photoemission spectrum of CuIr_2S_4 , *Radiat. Phys. Chem.* **75**, 2072 (2006).
- [12] J. Matsuno, T. Mizokawa, A. Fujimori, D. A. Zatselpin, V. R. Galakhov, E. Z. Kurmaev, Y. Kato, and S. Nagata, Photoemission study of the metal-insulator transition in CuIr_2S_4 , *Phys. Rev. B* **55**, R15979 (1997).
- [13] K. Kumagai, S. Tsuji, T. Hagino, and S. Nagata, NMR studies of superconductivity and metal-insulator transition in Cu spinel CuM_2X_4 ($M = \text{Rh}, \text{Ir}$ and $X = \text{S}, \text{Se}$), in *Spectroscopy of Mott Insulators and Correlated Metals*, Springer Series in Solid-State Sciences Vol. 119 (Springer, Berlin, Heidelberg, 1995), pp. 255–264.
- [14] T. Sasaki, M. Arai, T. Furubayashi, and T. Matsumoto, Band-structure theory for the insulating phase of the thio-spinel transition-metal compound, CuIr_2S_4 , *J. Phys. Soc. Jpn.* **73**, 1875 (2004).
- [15] S. Sarkar, M. De Raychaudhury, and T. Saha-Dasgupta, Density-functional study of the electronic and optical properties of the spinel compound CuIr_2S_4 , *Phys. Rev. B* **79**, 113104 (2009).
- [16] G. Cao, T. Furubayashi, H. Suzuki, H. Kitazawa, T. Matsumoto, and Y. Uwatoko, Suppression of metal-to-insulator transition and appearance of superconductivity in $\text{Cu}_{1-x}\text{Zn}_x\text{Ir}_2\text{S}_4$, *Phys. Rev. B* **64**, 214514 (2001).
- [17] R. Endoh, N. Matsumoto, S. Chikazawa, S. Nagata, T. Furubayashi, and T. Matsumoto, Metal-insulator transition in the spinel-type $\text{Cu}_{1-x}\text{Ni}_x\text{Ir}_2\text{S}_4$ system, *Phys. Rev. B* **64**, 075106 (2001).
- [18] J. R. Vegelius, K. O. Kvashnina, H. Hollmark, M. Klintonberg, Y. O. Kvashnin, I. L. Soroka, L. Werme, and S. M. Butorin, X-ray spectroscopic study of Cu_2S , CuS , and copper films exposed to Na_2S solutions, *J. Phys. Chem. C* **116**, 22293 (2012).
- [19] H. Sato, T. Nagasaki, K. Suekuni, H. I. Tanaka, A. Rousuli, S. Nakamura, N. Kawamura, X.-G. Zheng, T. Fujii, and T. Takabatake, Cu $2p - 1s$ x-ray emission spectroscopy of mineral tetrahedrite $\text{Cu}_{12}\text{Sb}_4\text{S}_{13}$, *Radiat. Phys. Chem.* **175**, 108148 (2020).
- [20] N. Kijima, H. Yashiro, J. Awaka, J. Akimoto, and S. Nagata, X-ray absorption spectroscopic analysis of CuIr_2S_4 , *J. Alloys Compd.* **480**, 120 (2009).
- [21] K. Hämäläinen, D. P. Siddons, J. B. Hastings, and L. E. Berman, Elimination of the Inner-Shell Lifetime Broadening in X-Ray-Absorption Spectroscopy, *Phys. Rev. Lett.* **67**, 2850 (1991).
- [22] N. Kawamura, N. Kanai, H. Hayashi, Y. H. Matsuda, M. Mizumaki, K. Kuga, S. Nakatsuji, and S. Watanabe, Lifetime-broadening-suppressed x-ray absorption spectrum of β - YbAlB_4 deduced from Yb $3d \rightarrow 2p$ resonant x-ray emission spectroscopy, *J. Phys. Soc. Jpn.* **86**, 014711 (2017).
- [23] F. Izumi and K. Momma, Three-dimensional visualization in powder diffraction, *Solid State Phenom.* **130**, 15 (2007).
- [24] F. W. Lytle, R. B. Greggor, and A. J. Panson, Discussion of x-ray-absorption near-edge structure: Application to Cu in the high- T_c superconductors $\text{La}_{1.8}\text{Sr}_{0.2}\text{CuO}_4$ and $\text{YBa}_2\text{Cu}_3\text{O}_7$, *Phys. Rev. B* **37**, 1550 (1988).
- [25] N. Kosugi, H. Kondoh, H. Tajima, and H. Kuroda, Cu K -edge XANES of $(\text{La}_{1-x}\text{Sr}_x)\text{CuO}_4$, $\text{YBa}_2\text{Cu}_3\text{O}_y$, and related Cu oxides. Valence, structure and final-state effects on $1s-4p\pi$ and $1s-4p\sigma$ absorption, *Chem. Phys.* **135**, 149 (1989).
- [26] N. L. Wang, G. H. Cao, P. Zheng, G. Li, Z. Fang, T. Xiang, H. Kitazawa, and T. Matsumoto, Optical study of the metal-insulator transition in CuIr_2S_4 , *Phys. Rev. B* **69**, 153104 (2004).
- [27] H. Gretarsson, J. Kim, D. Casa, T. Gog, K. R. Choi, S. W. Cheong, and Y.-J. Kim, X-ray induced electronic structure change in CuIr_2S_4 , *Phys. Rev. B* **84**, 125135 (2011).
- [28] The temperature range showing the hysteresis behavior is slightly below $T_{\text{MIT}} \sim 230$ K [1,2], which may be caused by temperature rising of the sample due to high intense synchrotron radiation. The temperature was monitored with a thermocouple attached to the copper sample holder. Actual temperature of the measured sample region would be about 10 K higher than the monitored temperature in comparison between the HERFD-XAS spectra in Fig. 3(b) and the electrical resistivity in Fig. 1(b).
- [29] H. Hayashi, R. Takeda, Y. Udagawa, and N. Kawamura, Lifetime-broadening-suppressed/free XANES spectroscopy by high-resolution resonant inelastic x-ray scattering, *Phys. Rev. B* **68**, 045122 (2003).
- [30] H. Hayashi, SIM-RIXS: a program to simulate resonant inelastic X-ray scattering, *X-Ray Spectrom.* **40**, 24 (2011).
- [31] J. Tulkki and T. Åberg, Behaviour of Raman resonance scattering across the K X-ray absorption edge, *J. Phys. B: Atom. Mol. Phys.* **15**, L435 (1982).
- [32] K. Okada and A. Kotani, Multiplet structures of Cu $2p$ -XPS in La_2CuO_4 , CuO and Cu halides, *J. Phys. Soc. Jpn.* **58**, 2578 (1989).
- [33] F. Di Benedetto, G. P. Bernardini, C. Cipriani, C. Emiliani, D. Gatteschi, and M. Romanelli, The distribution of Cu(II) and the magnetic properties of the synthetic analogue of tetrahedrite: $\text{Cu}_{12}\text{Sb}_4\text{S}_{13}$, *Phys. Chem. Miner.* **32**, 155 (2005).
- [34] K. Suekuni, K. Tsuruta, T. Ariga, and M. Koyano, Thermoelectric properties of mineral tetrahedrites $\text{Cu}_{10}\text{Ir}_2\text{Sb}_4\text{S}_{13}$ with low thermal conductivity, *Appl. Phys. Express* **5**, 051201 (2012).
- [35] H. I. Tanaka, K. Suekuni, K. Umeo, T. Nagasaki, H. Sato, G. Kutluk, E. Nishibori, H. Kasai, and T. Takabatake, Metal-semiconductor transition concomitant with a structural transformation in tetrahedrite $\text{Cu}_{12}\text{Sb}_4\text{S}_{13}$, *J. Phys. Soc. Jpn.* **85**, 014703 (2016).
- [36] T. Oda, M. Shirai, N. Suzuki, and K. Motizuki, Electronic band structure of sulphide spinels CuM_2S_4 ($M = \text{Co}, \text{Rh}, \text{Ir}$), *J. Phys.: Condens. Matter* **7**, 4433 (1995).